Scoria cones on Mars: detailed investigation of morphometry based on high-resolution Digital Elevation Models

Petr Brož[1,2], Ondřej Čadek[3], Ernst Hauber[4], Angelo Pio Rossi[5]

[1] Institute of Geophysics ASCR, v.v.i., Boční II/1401, 141 31, Prague, Czech Republic

[2] Institute of Petrology and Structural Geology, Faculty of Science, Charles University, Albertov 6, 128 00, Prague, Czech Republic

[3] Charles University, Faculty of Mathematics and Physics, Department of Geophysics, V Holešovičkách 2, 180 00, Prague, Czech Republic

[4] Institute of Planetary Research, DLR, Rutherfordstr. 2, 12489, Berlin, Germany

[5] Jacobs University Bremen, Campus Ring 1, 287 59, Bremen, Germany

9 figures

2 tables

Keywords: Mars, Mars surface, Volcanism, pyroclastic cone, scoria cone

Corresponding Author

Petr Brož
Institute of Geophysics
Czech Academy of Science (CAS) v.v.i
Boční II/1401
14131 Prague 4
Czech Republic

Key points:

- The morphometry of 28 Martian cones was investigated using HiRISE and CTX DEMs
- Ballistic analysis indicates that the cones were formed by Strombolian eruptions
- Despite variations in shape, cones are equivalent to terrestrial scoria cones

Abstract

We analyze the shapes of twenty eight hypothesized scoria cones in three regions on Mars, i.e. Ulysses and Hydraotes Colles and Coprates Chasma. Using available HiRISE and CTX Digital Elevation Models, we determine the basic morphometric characteristics of the cones and estimate from ballistic modelling the physical parameters of volcanic eruptions that could have formed them. When compared to terrestrial scoria cones, most of the studied cones show larger volumes (up to 4.2×10^9 m^3), larger heights (up to 573 m) and smaller average slopes. The average slopes of the Ulysses, Hydraotes and Coprates cones range between 7° and 25°, and the maximum slopes only rarely exceed 30°, which suggests only a minor role of scoria redistribution by avalanching. Ballistic analysis indicates that all cones were formed in a similar way and their shapes are consistent with an ejection velocity about two times larger and a particle size about twenty times smaller than on Earth. Our results support the hypothesis that the investigated edifices were formed by low energy Strombolian volcanic eruptions and hence are equivalent to terrestrial scoria cones. The cones in Hydraotes Colles and Coprates Chasma are on average smaller and steeper than the cones in Ulysses Colles, which is likely due to the difference in topographic elevation and the associated difference in atmospheric pressure. This study provides the expected morphometric characteristics of Martian scoria cones, which can be used to identify landforms consistent with this type of activity elsewhere on Mars and distinguish them from other conical edifices.

1. Introduction

Our knowledge of small-scale explosive volcanic cones on Mars thought to form by explosive volcanism has significantly increased in the recent years owing to a new generation of high resolution images that allow their identification [*Bleacher et al.*, 2007; *Keszthelyi et al.*, 2008; *Meresse et al*., 2008; *Lanz et al.*, 2010; *Brož and Hauber*, 2012; 2013]. Possible martian equivalents of terrestrial scoria cones were reported as parasitic cones on the flanks of large volcanoes [*Bleacher et al*., 2007; *Keszthelyi et al*., 2008] or as cone clusters forming volcanic fields [*Meresse et al*., 2008; *Lanz et al.*, 2010; *Brož and Hauber*, 2012; Fig. 1]. Although the interpretation of these edifices as scoria cones is mainly based on their apparent morphological similarity with terrestrial scoria cones, no detailed investigation of their morphometry using high-resolution data has yet been performed to support such a conclusion, with a partial exception for the Hydraotes Colles cone field [*Meresse et al*., 2008] and the Ulysses Colles cone field [*Brož and Hauber*, 2012; *Brož et al*., 2014].

It has been recognized that hypothesized martian scoria cones differ in size and shape from terrestrial scoria cones [*Meresse et al*., 2008; *Brož and Hauber* 2012]. Martian scoria cones are usually larger in basal diameter, higher, more voluminous by one to two orders of magnitude than their terrestrial counterparts, and the flanks do not exhibit slopes over 30° [e.g., *Brož and Hauber*, 2012; *Kereszturi et al.*, 2013]. The large basal diameter of the Martian cones can be explained by lower values of gravitational acceleration and atmospheric density on Mars than on Earth, which allow the scoria particles to be ejected further from the vent and deposited across a wider area than in terrestrial conditions [*McGetchin et al*., 1974; *Wood*, 1979; *Dehn and Sheridan*, 1990; *Wilson and Head*, 1994; *Brož et al*., 2014]. Although Martian cones are higher and have larger volumes than on Earth [*Brož and Hauber*, 2012], the amount of scoria material is typically not sufficient for the critical angle of repose to be attained over the main part of their flanks as it is common on Earth [*Riedel et al.*, 2003]. The principal mechanism of scoria cones formation on Mars is thus the ballistic emplacement of ejected particles which accumulate around the vent over time [*Brož et al*., 2014], rather than a redistribution of particles by avalanching processes typical of terrestrial scoria cones [*Riedel et al.*, 2003].

Previous studies dealing with the shape of scoria cones on Mars [*Meresse et al*., 2008; *Brož and Hauber*, 2012 and partially *Lanz et al.*, 2010] were based on data obtained through the High Resolution Stereo Camera (HRSC, [*Jaumann et al*., 2007]) and the Mars Orbiter Laser Altimeter (MOLA) Precision Experimental Data Records (PEDRs; [*Zuber et al.*, 1992; *Smith et al*., 2001]). Both instruments have only a limited horizontal resolution, which is optimal for investigating topographic features of a typical size of tens of kilometers or larger, but insufficient to provide detailed (~100 m - 1 km) information about small-scale features such as scoria cones (Fig. 2). This information is necessary for understanding the variability between cones and determining their morphometric characteristics. These are required for a quantitative comparison of the cones with similar features on Earth and other Martian conical edifices of various origins (e.g., mud volcanoes, pingos, rootless cones etc.; [*Burr et al.*, 2009]). In the present study, we use new high-resolution data from the High Resolution Imaging Science Experiment (HiRISE; *McEwen et al.*, 2007) and the Context Camera (CTX; [*Malin et al.*, 2007) which enable investigation of small edifices in unprecedented detail and quantitative analysis of their shapes (Fig. 2). Such an approach was tested previously by *Brož et al*. [2014] who investigated the shapes of two Martian scoria cones in Ulysses Colles using CTX Digital Elevation Models (DEMs) and one cone by HRSC DEMs.

Using the available high-resolution DEMs based on HiRISE and CTX stereo image pairs, we investigate the shapes of cones within three hypothesized volcanic fields (for details, see section 2) – Ulysses Colles (UC), Hydraotes Colles (HC) and Coprates Chasma (CC) where the existence of scoria cones has been suggested [*Meresse et al*., 2008; *Harrison and Chapman*, 2008; *Brož and Hauber*, 2012]. For each field, we first select a representative subset of cones that are well covered by HiRISE and/or CTX data. The topography of each cone is averaged with respect to the central axis, and the resultant axisymmetric structure is then characterized by several morphometric parameters, such as total volume, cone height and width, average and maximum slope etc. (for details, see section 4). Similar approaches have also been applied to terrestrial scoria cones [e.g., *Favalli et al*., 2009; *Kervyn et al*., 2012*; Kereszturi and Neméth*, 2012; *Kereszturi et al.*, 2012; for an overview see *Grosse et al*., 2012]. By comparing the parameters obtained for individual cones we evaluate the shape variability within each volcanic field and assess the degree of similarity among the fields. Finally, following the approach by *Brož et al*. [2014], which complements well the theoretical considerations of *Wilson and Head* [1994], we determine, for each cone, the ejection velocity and the particle size that best reproduce the observed shape of the cone, and again compare the results within and among the volcanic fields. The joint results of our morphometric analysis and numerical modeling are then discussed from the viewpoint of the formation mechanism of the cones and their volcanic origin.

2. Regional setting

The three fields considered in this study contain well-developed cones of various sizes with bowl-shaped central craters. The cones show only limited signs of modification by erosion. They are occasionally accompanied with short flow-like units associated with their flanks and/or craters. The cones occur as isolated edifices, or are grouped into small clusters where individual cones may coalesce or partially overlap each other. Their morphology and the fact they are associated with flow-like units suggest that the cones were formed by emplacement of material from the subsurface rather than by sediments from atmospheric deposition [*Meresse et al*., 2008;

Brož and Hauber, 2011]. Here, we briefly summarize the basic characteristics of the fields as described in previous studies.

2.1. Ulysses Colles

This volcanic field is situated in the Tharsis region at the south-eastern margin of Ulysses Fossae (Fig. 1a), a several-hundred-kilometer-long fault system trending mainly in north-south direction and fracturing a window of older crust which survived later resurfacing event(s) by younger lava flows. This field is located at a height of 4.5 km above the Martian datum over an area of about 80 × 50 km at the southern edge of Ulysses Fossae and it is formed by (at least) 29 volcanic cones [*Brož and Hauber*, 2012]. The cones are not distributed randomly; there is a cluster of 10 cones at the southern edge of this field. These cones have well-developed shapes and they seem to be well preserved. Three cones may be associated with flow-like features originating at the base and/or at the top of the cones. Unfortunately, only a small part of this field is covered by HiRISE or CTX stereo-pair images suitable for DEM production, hence our investigation of this field is based only on 7 cones.

2.2. Hydraotes Colles

This volcanic field is located in an area of jumbled assemblage of large, irregular blocks or mesas termed chaotic terrain [*Sharp*, 1973] on the eastern margin of Xanthe Terra (Fig. 1b). The area lies at the contact of two major large-scale complexes of fluid-eroded troughs outflow channels [*Baker et al*., 1992] (Simud and Tiu Vallis). The area is partly filled with large mesas separated by narrow valleys and by a basin with a smooth floor located 5 km below the Martian datum. Based on the inspection of HRSC and THEMIS data *Meresse et al*. [2008] identified about 40 cratered cones of various sizes and shapes in this basin, and divided them into three classes: basin cones, valley cones and small cones. The basin cones represent the largest edifices and are the subject of our investigation. These cones are predominantly located in the southern part of the chaotic terrain over a 40 × 30 km area. They have central craters and often form small sub-clusters separated by 5 km. The individual clusters are composed of cones which often partially overlap and/or are accompanied by flow-like units, interpreted by *Meresse et al*. [2008] as lava flows. Three clusters and one individual cone are covered by HiRISE stereo-pairs and two other cones are covered by CTX DEMs. This allows us to investigate 15 cones in this field.

2.3. Coprates Chasma

The largest field of hypothesized scoria cones is situated in the bottom part of the Coprates Chasma valley (Fig. 1c), one of the largest canyons in Valles Marineris, which extends over 1000 km. The cones and mounds are spread in a west-eastern direction over an area of 155 × 35 km, 5 km below the Martian datum on the floor of Coprates Chasma. Similarly to the cones in HC, the cones in CC sometimes form small clusters containing up to ten edifices, partly overlapping each other. The cones have been briefly mentioned by *Harrison and Chapman* [2008] as possible volcanic edifices; however, an origin associated with mud volcanism was also discussed and in the end chosen as the most plausible explanation. CTX and HiRISE images recently revealed previously unknown details [*Hauber et al.*, 2015] which seem to be consistent with a volcanic origin. At the time of writing this study, HiRISE stereo-pairs were available only for one cluster of cones. Our investigation focuses on 6 cones within this cluster, which represent only a small sample of this extensive field.

3. Topographic datasets

We used topographic data based on gridded digital elevation models (DEMs) derived from HiRISE (~30 cm/pixel, [*McEwen et al.*, 2007]) and CTX (5–6 m/pixel; [*Malin et al.*, 2007]) images. We computed the high-resolution DEMs from HiRISE and CTX stereo pairs using the methods described, e.g., in *Moratto et al*. [2010]. The image data were processed using the USGS Astrogeology image processing software Integrated System for Imagers and Spectrometers (ISIS3). The gridded HiRISE DEMs in UC, HC and CC have ground sampling distances of 0.53 m, 1.48 m and 3.82 m, respectively, while the resolution of CTX DEMs is 17.78 m. The overall absolute accuracy with respect to its position on the Martian surface is at the scale of a few meters. The relative (local) accuracy is typically higher because of the sub-meter resolution of the processed HiRISE data. The elevations of the DEMs are consistent with single shot data from MOLA PEDRs [*Garvin et al*., 2000]. In regions where both kinds of DEMs are available, we use only the HiRISE DEMs since they have a higher resolution than the CTX DEMs and hence provide a more detailed shape representation (Fig. 3). The spatial resolution of the HiRISE DEMs deteriorates in regions with a large amount of missing data (for an example, see Figs. 3a,b where the missing data are marked in white). These data gaps are associated with the process of DEM generation and affect the areas where an insufficient amount of matched points was produced before the interpolation of a DEM surface. Regions affected by too many data gaps were excluded from further analysis. Although the DEMs used in this study have relatively good spatial and vertical resolution (Fig. 3, bottom panel), small high-frequency variations in the topographic signal makes the accurate evaluation of the topographic slope difficult. The usual way to overcome this problem is to perform a spectral analysis of the signal and filter out the high-frequency noise in the spectral domain, or to remove the noise directly in the spatial domain using a moving average or smoothing method [e.g., *Kenney and Keeping*, 1962]. However, we find that neither of these methods works reliably when applied to the topographic data derived from HiRISE and CTX images because we are not able to distinguish a spurious high- and intermediate-frequency signal, arising from image processing, from the real small-scale topographic signal. The problem is obviously complex and its solution would require a better understanding of data errors. Here we simplify the problem by assuming that the studied edifices are axisymmetric. For each cone we define the center of symmetry as the geometrical center of the summit plateau and then we determine the average shape of the cone by averaging the topographic heights along the cross-sections passing through the center of symmetry. The angular step between the neighboring cross-sections is chosen to be 1 degree. This approach significantly reduces the noise in the topographic data and allows each cone to be described by a limited number of parameters (see next section). The parts of the cone with frequent data gaps and those where the axial symmetry is clearly disturbed (e.g., due to a lava flow, an irregularity of the bedrock topography or an overlap with another cone) are excluded from the averaging (see Table 1 for the list of sectors that have been considered).

4. Morphometric parameters

The morphometric properties studied for these cones are those that are commonly used for terrestrial scoria cones (Fig. 4a, for an overview see [*Grosse et al*., 2012]). These parameters are: the width or basal diameter of the cone (W_{CO}), the width of the crater (W_{CR}), the height of the cone (H_{CO}), the flank slope (α), and the volume. To determine these parameters for each cone we first correct for the influence of irregularities and compute the average shape (Fig. 4b) as described in section 3. The base level z_0 (marked by the dotted line in Fig. 4a), used to determine parameters W_{CO} and H_{CO}, is defined as the horizontal plane passing through the point where the slope of the average topographic profile exceeds one degree. This definition is independent of subjective factors and the results can be easily reproduced. It should be noted, however, that this approach may ignore far-reaching volcanic products [see, e.g., review by *Kereszturi and Németh,* 2012 for details] hardly detectable on topographic profiles and therefore may affect our volume estimates by underestimating the total amount of ejected material. The slope of each cone is described by a function α_z characterizing the dependence of slope α on relative height *h*,

$$\alpha_z(h) = 0.1 \int_{h-0.05}^{h+0.05} \alpha\ (h')dh', where\ h = \frac{z-z_0}{z_1-z_0}\ ,\ h \in \langle 0.05, 0.95\rangle \quad (1)$$

and by two constant parameters, the average slope and the maximum slope, defined as the average and maximum values of α_z, respectively (for meaning of parameter z_1, see Fig. 4a). Since the slope α is determined by numerical differentiation of the cone's shape, its accuracy strongly depends on the smoothness of the averaged topography. In the Coprates region, a high density of data gaps around the cones CC15 and CC22 and asymmetry of the cone CC20 do not allow the averaged shape to be reliably differentiated. The slope characteristics of these cones are therefore excluded from further analysis. In contrast, small errors in topographic height only weakly affect the evaluation of the volume and other parameters. The largest error in determining these parameters arises from the definition of the base level z_0 and violation of the assumption of symmetry. A similar problem has also been noted in studies focusing on terrestrial volcanic edifices [e. g., *Favalli et al*., 2009; *Kereszturi et al*., 2012]..

5. Results of morphometric analysis

We processed 8 stereo image pairs (5 HiRISE, 3 CTX) that enable the investigation of 28 conical structures in the three fields. 17 cones are covered by HiRISE DEMs and 11 by CTX DEMs. In all fields, only a subset of cones is considered since none of the fields is completely covered with stereo data of sufficient quality. As individual cones display morphological heterogeneity causing small variations in shape, we determine the average shape for each cone (for details, see section 3). These small variations may be caused by impact craters, sector collapses, migrations of feeder dikes, increase/decrease in explosivity and, partly, erosion.

Examples of such variations are shown in Figs. 4b and 5a-c for the case of a cone in the Hydraotes region. Additionally, it is known from Earth that similar variations may be associated with syn-eruptive variations of eruption styles [*Kereszturi and Neméth*, 2012; *Kereszturi et al.*, 2012] and it is reasonable to expect that the same is also valid for Mars. The topographic height of the cone depends not only on the distance from the center but also on azimuth, suggesting variations in particle distribution and deposition over the entire perimeter of the cone – see Fig. 4b where topographic profiles along two cross-sections are compared with the resultant average shape. As obvious from the slope map (Fig. 5b), the southern part of the cone is steeper than the northern one, while the western part is affected by sector collapse and/or impact craters (Fig. 5c).

The parameters of the cones obtained after averaging are summarized in Table 1 and depicted in Fig. 6. In general, the size of the cones varies among the three investigated fields (Fig. 6a). The cones in UC have, on average, the largest mean basal diameter, the widest central crater and also include the highest edifices (Fig. 6b) with mean values of 4080 m, 650 m and 320 m, respectively. The cones in HC are mostly smaller than the cones in UC, with mean basal diameter, crater width and cone height of 1880 m, 290 m and 190 m, respectively. The statistically smallest edifices are found in the CC region; but their mean characteristics (W_{CO}=1490 m, W_{CR}=290 m and H_{CO}=160 m) do not differ much from those of the HC cones.

The slopes and volumes of the cones vary significantly from cone to cone within individual fields and also among the fields. As the cones in UC are largest and highest, they include the most voluminous edifices (Fig. 6c). However, even the largest cones in this region show smaller average slopes than the steepest edifices in HC and CC (Fig. 6d). The average slopes $\bar{\alpha}$ in UC range between 7° and 18° with corresponding cone volumes between 1.5×10^8 m^3 and 4.2×10^9 m^3, while the cones in HC and CC have similar or even larger average slopes (13° – 24°), but their volumes range from 2.1×10^7 m^3 to only 4.6×10^8 m^3 (see also Tab. 1). The cones in HC and CC are thus similar in volume to terrestrial scoria cones which are on average formed by 4.6×10^7 m^3 of material (determined from 986 edifices, data from *Pike* [1978] and *Hasenaka and Carmichael* [1985]).

The slope α_z (eq. 1) is not uniform along the entire length of a cone flank but changes with height (Fig. 7). It is lowest at the cone's bottom and increases with height, reaching a maximum between normalized height values of 0.6 and 0.8. Then the slope again decreases around the edge of the crater. Note that in all plotted cases (8 cones in HC, 7 cones in UC and 3 cones in CC) the slope is always smaller than the angle of repose (~30°; *Kleinhans et al*., [2011]).

5.1. Ballistic emplacement models

To assess the mechanism of cone formation, we used the numerical code developed by *Brož et al.* [2014] which is able to track the ballistic trajectories and trace the cumulative deposition of repeatedly ejected particles during low-energy Strombolian eruptions. This code can be used to reconstruct the shapes of ballistically emplaced volcanic edifices (e.g., scoria cones) and hence to confirm or disprove the formation mechanism of investigated cones. *Brož et al.* [2014] have applied this approach to study three selected cones (UC1, UC2 and UC8) in the UC region. Using log-normal statistical distributions of ejection velocities and particle sizes with the same standard deviations as on the Earth and assuming that the density of air at the time of eruption was the same as today, they found that the shapes of the cones are consistent with a Strombolian origin, provided that the mean ejection velocity was about two times larger and the particle size about ten twenty smaller than on Earth.

Here we repeat the same numerical experiment but using much larger and more accurate topographic datasets. For each of the 28 cones considered in this study we determine the mean particle size and the mean ejection velocity that best predict the average shape of the cone. We use the same parameters as in *Brož et al.* [2014], see Table 2, except that we prescribe a higher atmospheric density in HC and CC (0.023 kg/m^3) than in UC (0.010 kg/m^3) and consider only the wide ejection cone (0-45°), which is likely on a terrestrial body with a low atmospheric pressure [*Glaze and Baloga*, 2000; *Wilson and Head*, 2007]. The large difference in the air density is associated with the different elevation of the fields, about 9.5 km. Since atmospheric drag is proportional to the air density, the ballistic range in HC and CC should be smaller than in UC, and the HC and CC cones should be steeper than their UC counterparts.

The results of our modeling are summarized in Table 1 and illustrated in Fig. 8 where the observed topographies are compared with our ballistic predictions for several selected cones. Our results suggest that the ballistic model is not only able to reconstruct the cones rather well in all three fields but also that the shapes of most of them can be explained using similar values of ejection velocity and particle size, even though the cones have various sizes and volumes and are located in regions with different air drag. The agreement between the observed and predicted topography, expressed as the L^2 norm distance between the topographic curves divided by the width of the cone, is given in the last column of Table 1. The vertical distance between the observed and predicted topography ranges from 1.2 to 21.8 m, with an average value of 9 m. The predicted values of the ejection velocities range by a factor of three, from 45 to 135 m/s, but 50% of them lie in the narrow interval between 82 and 102 m/s. The particle size that best predicts the observation is between 1 and 2 mm, except for two cones where it reaches 4-5 mm. The mean values of the best-fitting ejection velocity and particle size obtained for individual fields are, respectively, ~100 m/s and 1.8 mm for UC, 91 m/s and 1.8 mm for HC, and 84 m/s and 1.3 mm for CC. We note that our ballistic inversion is sensitive to the ratio between particle size and air density, but not to the particle size itself. To obtain the particle sizes given above, we had to assume particular values of air density corresponding to the time of eruption. Since the ages of individual cone fields are not known with sufficient accuracy and the evolution of the atmosphere is poorly constrained, we used the current atmospheric density, corrected for the altitude of individual fields, namely 0.010 kg/m^3 for UC and 0.023 kg/m^3 for HC and CC (based on Mars Global Surveyor spacecraft data of April 1996 [*Glenn Research Center*, 2015]).

6. Discussion

6.1. Igneous or mud volcanism?

The investigation of the origin of Martian surface landforms is complicated by the lack of in-situ data which could provide conclusive evidence of their mode of formation. The available remote sensing data provide only limited insight into the formation of surface features, and they can usually be interpreted in several different ways [e.g., *Beven*, 1996]. This is also the case for the cones in HC and CC, for which two different explanations have been suggested: igneous volcanism and mud volcanism [*Meresse et al*., 2008; *Harrison and Chapman*, 2008]. The igneous volcanic scenario assumes that the investigated features are scoria cones formed by tephra particles produced via Strombolian eruptions by magma degassing and associated fragmentation [*Parfitt and Wilson*, 2008]. Strombolian eruptions are often accompanied by the effusion of lava flows, which would explain the flow-like features associated with the cones. On the other hand, a mud volcanic scenario assumes that the cones are mud volcanoes produced due to the mobilization of fine-grained material from deeper crustal levels by a mixture of liquid and gases

[*Skinner and Mazzinni*, 2009]. This mobilization may lead to the eruption of ascending mud and subsequent deposition, but also to mud effusion in the form of mud flows. It is difficult to distinguish between these two scenarios as both fields are located in areas where water played or may have played an active role, and both mechanisms may form conical landforms associated with central craters and flow units. However, the existence of the cones in UC may help to solve this problem. Located in an elevated area of a heavily fractured crust where the existence of a stable aquifer and/or a source of mud is highly unlikely, this field can hardly be associated with mud volcanism, and an explanation in terms of Strombolian volcanism is much more plausible [*Brož and Hauber*, 2012]. The shape similarity (or dissimilarity) between the cones in this region and those in HC and CC may thus provide a key to understanding how the features in HC and CC were formed. Of course, this assumption is only valid if the cones still record information about the original shape and they were not significantly affected by erosion. Although erosion may have affected the flank slopes, this effect is considered small and did most likely not alter the original slopes significantly. First, the inspection of cone flanks does not reveal major erosive features such as rills or gullies. The only exceptions are the eastern flanks of cones in HC which seem to be partly furrowed and are therefore excluded from our analyses. Second, erosion rates on Mars are extremely small when averaged over the last 3 Ga (10^{-6} to 10^{-4} m/Myr; [*Golombek et al.*, 2014, 2015]). While some easily erodible material such as the interior layered deposits in Valles Marineris may be subject to higher erosion rates (1200-2300 nm/yr; *Grindrod and Warner* [2014]), the relative young Amazonian ages [Brož and Hauber, 2012; Hauber et al., 2015] of the investigated cones would limit the total amount of erosion that would have occurred. Moreover, it is not expected that erosion rates at the time of cone formation were significantly higher than today, as the average paleopressure of the Martian atmosphere was most likely low during the entire Amazonian [e.g., *Kite et al*., 2014].

6.2. Insight from ballistic modeling

As already mentioned, the cones in all three investigated fields can be described as conical edifices with a central crater (Fig. 1). Their slopes seem to be formed by a fine-grained material with a smooth texture, and some of them are accompanied by flow-like units with lobate edges and a rough texture. Therefore, it is reasonable to expect that a similar physical mechanism was responsible for their formation. However, when the shapes of the cones are compared quantitatively (section 5), the similarity of the fields becomes less obvious. As shown in Fig. 6 and Table 1, individual cones show variations in size, height, volume and slope, and, on the morphometric graphs, they do not form one homogenous cluster with a clear linear trend as common for fresh scoria cones on Earth [*Porter*, 1972; *Wood*, 1980]. Instead, two trends may be distinguished: one formed by the cones in HC and CC showing a significant overlap in all measured parameters (Fig. 6), and the other consisting of the cones in UC following a different trend.

The close agreement in the morphometries of the cones in HC and CC supports the concept that both fields were formed by the same or a similar physical mechanism. On the other hand, the morphological differences between the cones in these two fields and those in UC may raise doubts whether the HC and CC cones were formed by the same process as the cones in UC, which are likely of volcanic origin [*Brož and Hauber*, 2012]. The analysis of the cones in terms of ballistic modeling however shows that the difference between UC on one side and HC and CC on the other is only apparent. Despite the obvious morphological differences, the cones in all three fields can be explained by the same ballistic model with the same or similar ejection velocity and particle size distributions. This result suggests that the edifices in the three regions are scoria cones which were formed by the same physical process, though under different atmospheric pressure, rather than mud volcanoes which are known to be formed on Earth mainly by effusive activity [*Kholodov*, 2002].

The ballistic model provides a simple explanation of the morphological differences between the cones in UC and those in HC and CC, indicating that these differences are associated with the different elevations of the sites, rather than with different processes of cones' formation. At present, the atmospheric density in HC and CC is a factor of about 2.3 larger than in UC. Although the fields may have different ages, it is likely that they were formed during the last one billion years [*Brož and Hauber*, 2012; *Hauber et al.*, 2015] when the atmospheric pressure was already low [*Lammer et al*., 2013]. One can thus assume that the difference in the density of air between the sites at the time of their origin was similar to that at present. The atmospheric drag is linearly proportional to the air density and hence is about 2.3 times smaller in UC than in other two regions. The ballistic range of ejected particles increases as the atmospheric drag decreases [*Brož et al*., 2014], and the ejected material is thus deposited over a wider area in UC than in HC and CC. For the same volume of ejected material, the cones in HC and CC must therefore be narrower and steeper than those in UC, which is well illustrated in Fig. 6. But even in the case of HC and CC, the atmospheric friction is significantly (about 50 times) lower than on Earth so that the ejected material is dispersed over a larger area than under terrestrial conditions [*Brož et al*., 2014]. The dispersion of particles on Mars is further enhanced by low gravity. As a consequence, the slopes angles of the cones are supply-limited and do not reach the angle of repose as is common for scoria cones on Earth which explains why the scoria cones on Mars do not morphologically resemble their terrestrial analogues. While the shape of the Martian scoria cones is only determined by ballistic emplacement, the shape of the cones on Earth is also influenced by avalanche redistribution of the ejected material occurring after the cone reached the angle of repose [*Riedel et al*., 2003], and also by other factors such as pre-eruptive surface inclination, vent migration, lava outlflow with associated crater breaching, and/or diversity of pyroclastic rocks accumulation in the flanks of volcanoes [*Kereszturi and Németh,* 2012; *Kereszturi et al.*, *2012*].

6.3. Comparison of scoria cones on Earth and Mars

The differences in evolution of scoria cones on Earth and Mars are illustrated in Fig. 9. At the beginning (stages 1 and 2 in Fig. 9), both cones grow in a similar manner, gradually increasing in height and slope angle. Because of the differences in the ballistic range, the ejected particles are deposited over a much smaller area on Earth than on Mars and, for the same amount of ejected material, the terrestrial cone is thus steeper than the Martian one. Once the angle of repose (~30°) on Earth is reached (stage 3, Fig. 9 left), the slope angle stops increasing and it remains stable during the rest of its evolution. Further growth is accommodated by an increase in cone width [*McGetchin et al.*, 1974; *Kereszturi and Németh,* 2012]. To summarize, the evolution of a scoria cone on Earth has two main phases: The first (stages 1 and 2 in Fig. 9) is characterized by a positive correlation between height and slope angle and, to first approximation, by a constant basal diameter. In the second phase (stages 3 to 5 in Fig. 9), the slope does not change and the correlated parameters are height and basal diameter. As a consequence, the terrestrial population of scoria cones can be classified into two main groups. The first group consists of small cones corresponding to the first phase and showing a correlation between angle of slope and height due to the ballistic deposition and/or fallout from turbulent jets [*Riedel et al*., 2003; *Valentine et al*., 2005]. The second (and much more numerous) group includes large cones that reached the second phase and show a correlation between height and basal diameter due to the avalanching [*Bemis et al*., 2011]. The cones of this group have the same or very similar shapes even though they have different volumes and their basic physical characteristics (ejection velocity, particle size etc.) may vary significantly from cone to cone. Thanks to this self-similarity, scoria cones on Earth can be easily identified, but it is difficult to trace back the physical conditions at the time of eruption (e.g., ejection velocity).

The evolution of scoria cones on Mars is different in that none of the studied cones reaches the second phase and even that the second phase has not been observed elsewhere on Mars yet. The cones were built by ballistic deposition only and, in spite of large volumes of ejected material, their flank slopes did not attain the angle of repose because the area over which the material was deposited was very large. Each investigated scoria cone on Mars thus contains a record of the specific physical conditions at the time of eruption which can be, at least partly, inferred from its shape. This also explains the wide variety of shapes (Fig. 6 and 7) observed in the three regions studied in this paper. It should be noted that this explanation is valid only if the role of ballistic emplacement is dominant and one can neglect other effects that may have influenced the shapes of cones. As shown by numerous studies on explosive volcanism on Earth [e.g., *Riedel et al*., 2003; *Calvari and Pinkerton,* 2004; *Valentine et al*., 2005; *Vanderkluysen et al*., 2012], fire fountaining and deposition of material from ash jets and/or from neutral buoyant plumes can also contribute to the formation of terrestrial scoria cones. It is difficult to assess how significant these processes were on Mars. It should therefore be kept in mind that our present approach may represent a considerable simplification of the processes that formed the Martian scoria cones.

We find that the volumes of the investigated cones (Fig. 6c) are generally larger by one to two orders of magnitude than is typical of terrestrial scoria cones [*Brož et al*., 2014] for which the average volume is 0.046 km^3 (determined from 986 edifices, data from [*Pike,* 1978] and

[*Hasenaka and Carmichael*, 1985]). This suggests that monogenetic volcanism on Mars had to be more voluminous in the past than on Earth. Unfortunately, a direct link between the size of cone and the total amount of erupted material is not easy to establish and our estimates of magma volumes are only approximate. On Earth, the size of the scoria cone is a function of the amount of magma erupted in the close vicinity of the vent and does not necessarily correspond to the total amount of magma reaching the surface. This is because a large amount of fine grained material fragmented from magma during the volcanic eruption can be transported by a neutrally buoyant volcanic cloud and deposited far away from the main body of the cone [*Bemis et al*., 2011]. One can expect that some material was also transported away from the immediate vicinity of the Martian cones [*Brož et al.*, 2014] by the neutrally buoyant volcanic cloud. Therefore, the measured volumes (Table 1 and Fig. 6c) may underestimate the total volume of erupted material as they represent only the material contained in the cone itself. Such an underestimate is also common for terrestrial scoria cones if their volume is calculated in a similar way used in this study [e.g., *Favalli* et al., 2009; *Bemis et al*., 2011; *Kereszturi et al.*, 2012]; however, this underestimate may be avoided by using isopachs, or several continuous LiDAR measurements [*Fornaciai et al*., 2010], which are, however, not available on Mars.

A comparison of the heights of volcanoes and the corresponding volumes (Fig. 6 and Table 1) shows that the largest (H_{CO} > 400 m) cones are all from UC. The existence of large-size volcanoes in UC and their absence in HC and CC is a puzzling problem that cannot be answered by ballistic modeling. Although the high-resolution DEMs are available only for limited parts of HC and CC, it is unlikely that large edifices of similar size as in UC escaped detection since both fields are covered with CTX data. The anomalously large volume of the UC cones must thus be attributed to local geological setting. As already mentioned in section 2.1, the UC cones are located in a region of large crustal extension which occurred concurrently with the volcanic activity [see also *Brož and Hauber*, 2012]. The large crustal extension in UC could lead to a larger extent of decompression melting and hence to the production of larger batches of magma ascending to the surface than in HC and CC.

For each cone we also determine the W_{CR}/W_{CO} and H_{CO}/W_{CO} ratios (Table 1 and Fig. 6a,b). These two ratios have been widely used in terrestrial and planetary science since they are considered to have the potential to distinguish different landforms [e.g., *Wood*, 1980; *Burr et al*., 2009; *Brož and Hauber*, 2012; 2013; *Noguchi and Kurita*, 2015]. The average values of these ratios for terrestrial scoria cones are 0.4 and 0.17, respectively [*Porter*, 1972; *Wood*, 1980]. On Mars, W_{CR}/W_{CO} ranges from 0.05 to 0.34 with an average of 0.17. The large differences between the values of W_{CR}/W_{CO} of Martian scoria cones may be associated with variations in explosivity caused by a varying amount of released magma gases and/or water in liquid and/or solid phase [*Sheridan and Wohletz*, 1983; *Wohletz and Sheridan*, 1983]. The variable presence of gases and/or water would result in a variable intensity in explosivity and thus in variation of crater width [*Bemis et al*., 2011]. The W_{CR}/W_{CO} ratios found in this study are significantly lower than those seen in scoria cones on Earth. This may be related to the method of calculating W_{CR} which tends to underestimate the crater width in cases where the crater is asymmetric. For example, if the crater has a shape of an ellipse with semi-axes a and b, $a>b$, the arithmetic averaging of topographic profiles (see section 3) gives W_{CR} close to 2b rather than $a+b$. Comparison of the values of W_{CR} in Table 1 with those inferred from planform imagery (Fig. 1) suggests that the value of W_{CR}/W_{CO} may indeed be underestimated in some cases but not enough to explain the factor of 2 difference between the Martian and terrestrial values. This indicates that the issue of small craters on Mars is a real phenomenon which requires further investigation. Our present ballistic model does not provide enough insight into this problem because the central part of the cones is usually approximated with a lower accuracy than the flanks (Fig. 8). The H_{CO}/W_{CO} ratio varies from 0.03 to 0.14 with the average value being 0.10. This value is significantly smaller than on Earth which can be accounted for by the differences in formation mechanisms – ballistic deposition on Mars and avalanching on Earth.

7. Conclusions

Our study provides a coherent set of morphometric characteristics of 28 conical Martian edifices from three regions – Ulysses Colles, Hydraotes Colles and Coprates Chasma. These characteristics are derived from newly available high-resolution DEMs based on HiRISE and CTX stereo-pair images. For each cone we carefully reconstruct its average (axisymmetric) shape and determine the basic morhometric parameters – volume, height, basal width, crater width and slope.

The parameters obtained for the cones in HC and CC show similar distributions which suggests that both fields were created by the same geological process. The cones in UC, which have been interpreted by *Brož and Hauber* [2012] as scoria cones, form an independent trend on morphometric graphs and their characteristics differ from those in HC and CC – the cones are more voluminous and have smaller average slope angles than the cones in the other two regions. Using our numerical ballistic model, we show that the difference between the cones in UC and those in HC and CC is only apparent. In spite of obvious morphological differences, the cones in all three fields can be explained by the same ballistic model with the same ejection velocity and particle size distributions. This result suggests that the edifices in all three regions are scoria cones which were formed by the same physical process. The differences in the shape of the cones in UC and those in HC and CC are associated with different elevations of the sites and can be explained by different values of atmospheric drag. The values of ejection velocity and particle size inferred from the topographic data are in agreement with the theoretical predictions by *Wilson and Head* [1994], who argued for stronger magma fragmentation and higher ejection velocities on Mars in comparison with the Earth.

Our results support the hypothesis that Martian scoria cones differ in shape from the terrestrial cones due to the different mechanism of flank formation [*Brož et al*., 2014]. Because of a long ballistic range, the slopes of scoria cones on Mars never reach the angle of repose and their shapes are fully determined by ballistic deposition – in contrast to the Earth where the subsequent avalanche redistribution plays the dominant role. As a consequence, Martian scoria cones show a wide variety of sizes and slope angles, corresponding to different stages of the scoria cone's growth and different volumes of ejected material.

The set of morphological characteristics derived in this study can further be used for comparative studies of other conical edifices on Mars, such as pingos [*Burr et al*., 2009], rootless cones [*Noguchi and Kurita*, 2015], mud volcanoes [*Skinner and Mazzini*, 2009] or tuff rings and tuff cones [*Brož et al*., 2013], and can help to overcome the uncertainties associated with using terrestrial morphometric data which correspond to different environmental conditions and possibly include effects that are not relevant to Mars. As shown in our study, the role of environmental conditions is also important and should be taken into account when comparing similar geomorphological features at significantly different altitudes.

Acknowledgements

Discussions with Frank Scholten helped to assess the accuracy of DEMs. Topographic data used in this study are publicly available at doi:10.5281/zenodo.18590. We thank the responsible editor, David Baratoux, and two anonymus reviewers for constructive comments and inspiring suggestions. This study was supported by grant No. 580313 of the Charles University Science Foundation (GAUK).

References

Baker, V.R., M. H. Carr, V. C. Gulick, C. R. Williams, and M. S. Marley (1992), Channels and valley networks, in: Kieffer H. H, B. M. Jakosky, C. W. Snyder, and M. S. Matthews (eds): Mars. University of Arizona Press, Tucson, 493–522.

Bemis, K., J. Walker, A. Borgia, B. Turrin, M. Neri, and C. Swisher (2011), The growth and erosion of cinder cones in Guatemala and El Salvador: models and statistics, Journal of Volcanology and Geothermal Research, 201(1–4), 39–52, doi: 10.1016/j.jvolgeores.2010.11.007.

Beven, K. (1996), Equifinality and Uncertainty in Geomorphological Modelling. In: The Scientific Nature of Geomorphology, Proc. 27th Binghampton Symp. Geomorphology, B.L. Rhoads and C.E. Thorn (eds.), 289-313, Wiley.

Bleacher, J. E., L. S. Glaze, R. Greeley, E. Hauber, S. M. Baloga, S. E. H. Sakimoto, D. A. Williams, and T. D. Glotch (2009), Spatial and alignment analyses for a field of small volcanic vents south of Pavonis Mons and implications for the Tharsis province, Mars, Journal of Volcanology and Geothermal Research, 185, 96–102, doi: 10.1016/j.jvolgeores.2009.04.008.

Brož, P., and E. Hauber (2012), A unique volcanic field in Tharsis, Mars: Pyroclastic cones as evidence for explosive eruptions, Icarus, 218, 1, 88–99, doi:10.1016/j.icarus.2011.11.030.

Brož, P., and E. Hauber (2013), Hydrovolcanic tuff rings and cones as indicators for phreatomagmatic explosive eruptions on Mars, Journal of Geophysical Research: Planets, 118, 1656–1675, doi: 10.1002/jgre.20120.

Brož. P., O. Čadek, E. Hauber, and A. P. Rossi (2014), Shape of scoria cones on Mars: insights from numerical modeling of ballistic pathways, Earth and Planetary Science Letters, 406, 14–23, doi: 10.1016/j.epsl.2014.09.002.

Burr, D. M., K. L. Tanaka, and K. Yoshikawa (2009), Pingos on Earth and Mars, Planetary and Space Science, 57(5-6), 541–555, doi: 10.1016/j.pss.2008.11.003.

Calvari, S., and H. Pinkerton (2004), Birth, growth and morphologic evolution of the 'Laghetto' cinder cone during the 2001 Etna eruption, Journal of Volcanology and Geothermal Research, 132, 225–239, doi10.1016/S0377-0273(03)00347-0.

Dehn, J., and M. F. Sheridan (1990), Cinder cones on the Earth, Moon, Mars, and Venus: A computer model, 21st Lunar and Planetary Institute Science Conference, #270 (abstract).

Favalli, M., D. Karatson, F. Mazzarini, M.T. Pareschi, and E. Boschi, (2009), Morphometry of scoria cones located on a volcano flank: a case study from Mt. Etna (Italy), based on high-resolution LiDAR data, Journal of Volcanology and Geothermal Research, 186, 320–330, doi:10.1016/j.jvolgeores.2009.07.011.

Fornaciai, A., B. Behncke, M. Favalli, M. Neri, S. Tarquini, and E. Boschi, (2010), Detecting short-term evolution of Etnean cinder cones: a LIDAR-based approach. Bulletin of Volcanology doi:10.1007/s00445-010-0394-3.

Garvin, J. B., S. E. H. Sakimoto, J. J. Frawley, and C. C. Schnetzler (2000), North polar region craterforms on Mars: Geometric characteristics from the Mars Orbiter Laser Altimeter, Icarus, 144, 329–352, doi: 10.1006/icar.1999.6298.

Glaze, L. S., and S. M. Baloga (2000), Stochastic-ballistic eruption plumes on Io, Journal of Geophysical Research: Planets, 105, 17579–17588, doi: 10.1029/1999JE001235.

Glenn Research Center (2015), "Mars Atmospheric Model - Metric Units". Web, 10/08/2015.

Golombek, M. P., et al. (2006), Erosion rates at the Mars Exploration Rover landing sites and long-term climate change on Mars. J. Geophys. Res. 111, E12S10, doi: 10.1029/2006JE002754.

Golombek, M. P., N. H. Warner, V. Ganti, M. P. Lamb, T. J. Parker, R. L. Fergason, and R. Sullivan (2014), Small crater modification on Meridiani Planum and implications for erosion rates and climate change on Mars. J. Geophys. Res. Planets 119, 2522-2547, doi: 10.1002/2014JE004658.

Golombek, M. P., N. H. Warner, V. Ganti, and M. P. Lamb (2015), Degradation of small craters on Meridiani Planum and erosion rates on Mars. Lunar Planet. Sci. 46, LPI Contribution No. 1832, abstract 1610.

Grindrod, P. M., and N. H. Warner (2014), Erosion rate and previous extent of interior layered deposits on Mars revealed by obstructed landslides. Geology 42(9), 795-798, doi: 10.1130/G35790.1.

Grosse P., B. van Wyk de Vries, P. A. Euillades, M. Kervyn, and I. Petrinovic (2012), Systematic morphometric characterization of volcanic edifices using digital elevation models, Geomorphology, 136, 114–131, doi:10.1016/j.geomorph.2011.06.001.

Hasenaka, T., and I. S. E. Carmichael (1985), The cinder cones of Michoacán–Guanajuato, central Mexico: their age, volume and distribution, and magma discharge rate, Journal of Volcanology and Geothermal Research, 25, 104–124, doi: 10.1016/0377-0273(85)90007-1.

Harris, A. J. L, M. Ripepe, and E. A. Hughes (2012), Detailed analysis of particle launch velocities, size distributions and gas densities during normal explosions at Stromboli, Journal of Volcanology and Geothermal Research, 231–232, 109–131 doi:10.1016/j.jvolgeores.2012.02.012.

Harrison, K. P, and M. G. Chapman (2008), Evidence for ponding and catastrophic floods in central Valles Marineris, Mars, Icarus 198, 351–364, doi: 10.1016/j.icarus.2008.08.003.

Hauber, E., P. Brož, A. P. Rossi, and G. Michael (2015), A Field of Small Pitted Cones on the Floor of Coprates Chasma, Mars: Volcanism Inside Valles Marineris?, 46th Lunar and Planetary Institute Science Conference, #1476 (abstract).

Jaumann, R., et al. (2007), The high-resolution stereo camera (HRSC) experiment on Mars Express: Instrument aspects and experiment conduct from interplanetary cruise through the nominal mission, Planetary and Space Science, 55, 928–952, doi: 10.1016/j.pss.2006.12.003.

Kenney, J. F., and E. S. Keeping (1962), Mathematics of Statistics, 3rd edition, Princeton, NJ: Van Nostrand.

Kereszturi, G., and K. Németh (2012), Monogenetic basaltic volcanoes: genetic classification, growth, geomorphology and degradation. In: Németh, K. (Ed.), Updates in Volcanology — New Advances in Understanding Volcanic Systems, 3–88, doi: 10.5772/51387.

Kereszturi, G., G. Jordan, K. Németh, and J. F. Doniz-Paez (2012), Syn-eruptive morphometric variability of monogenetic scoria cones, Bulletin of Volcanology, 74(9), 2171–2185, doi: 10.1007/s00445-012-0658-1.

Kereszturi G., A. Geyer, J. Martí, K. Németh, and F. J. Dóniz-Páez (2013), Evaluation of morphometry-based dating of monogenetic volcanoes—a case study from Bandas del Sur, Tenerife (Canary Islands), Bulletin of Volcanology, 75:734, doi 10.1007/s00445-013-0734-1.

Kervyn, M., G. G. J. Ernst, J.-C. Carracedo, and P. Jacobs, P. (2012), Geomorphometric variability of "monogenetic" volcanic cones: evidence from Mauna Kea, Lanzarote and experimental cones, Geomorphology, 136, 59–75, doi:10.1016/j.geomorph.2011.04.009.

Keszthelyi, L., W. Jaeger, A. McEwen, L. Tornabene, R. A. Beyer, C. Dundas, and M. Milazzo (2008), High Resolution Imaging Science Experiment (HiRISE) images of volcanic terrains from the first 6 months of the Mars Reconnaissance Orbiter primary science phase, Journal of Geophysical Research, 113, E04005. doi:10.1029/ 2007JE002968.

Kleinhans, M. G., H. Markies, S. J. de Vet, A. C. in 't Veld, and F. N. Postema (2011), Static and dynamic angles of repose in loose granular materials under reduced gravity, Journal of Geophysical Research, 116, E11004, doi:10.1029/2011JE003865.

Kholodov, V. N. (2002), Mud volcanoes: Distribution regularities and genesis (Communication 2. geological–geochemical peculiarities and formation model), Lithol. Miner. Resour., 37, 293–310, doi:10.1023/A:1019955921606.

Lammer, H., et al. (2013), Outgassing history and escape of the Martian atmosphere and water inventory, Space Science Reviews, 174 (1–4), 113–154, doi: 10.1007/s11214-012-9943-8.

Lanz, J. K., R. Wagner, U. Wolf, J. Kröchert, and G. Neukum, (2010), Rift zone volcanism and associated cinder cone field in Utopia Planitia, Mars, Journal of Geophysical Research, 115, E12019, doi:10.1029/2010JE003578.

Malin, M. C., et al. (2007), Context camera investigation on board the Mars Reconnaissance Orbiter, Journal of Geophysical Research, 112, E05S04, doi: 10.1029/2006JE002808.

McEwen, A. S., et al. (2007), Mars Reconnaissance Orbiter's High Resolution Imaging Science Experiment (HiRISE), Journal of Geophysical Research, 112, E05S02, doi: 10.1029/2005JE002605.

McGetchin, T. R., M. Settle, and B. A. Chouet (1974), Cinder cone growth modelled after North East crater, Mt Etna, Sicily, Journal of Geophysical Research, 79, 3257–3272, doi: 10.1029/JB079i023p03257.

Meresse, S., F. Costard, N. Mangold, P. Masson, G. Neukum, and the HRSC Co-I Team (2008), Formation and evolution of the chaotic terrains by subsidence and magmatism: Hydraotes Chaos, Mars, Icarus, 194, 487–500, doi: 10.1016/j.icarus.2007.10.023.

Moratto, Z. M., M. J. Broxton, R. A. Beyer, M. Lundy, and K. Husmann (2010), Ames Stereo Pipeline, NASA's Open Source Automated Stereogrammetry Software. In: 41st Lunar and Planetary Institute Science Conference, #2364 (abstract).

Noguchi R., and K. Kurita (2015), Unique characteristics of cones in Central Elysium Planitia, Mars, Planetary and Space Science, 111, 44–54, doi:10.1016/j.pss.2015.03.007.

Parfitt, E.A., and L. Wilson, (2008), Fundamentals of Physical Volcanology. Blackwell, Oxford. 256 p.

Pike, R. J. (1978), Volcanoes on the inner planets: Some preliminary comparisons of gross topography. Proc. Lunar Sci. Conf. IX, 3239–3273 (abstract).

Porter, S.C. (1972), Distribution, morphology, and size frequency of cinder cones on Mauna Kea Volcano, Hawaii, Geological Society of America Bulletin, 83, 3607–3612, doi: 10.1130/0016-.

Riedel, C., G. G. K. Ernst, and M. Riley (2003), Controls on the growth and geometry of pyroclastic constructs, Journal of Volcanology and Geothermal Research, 127, 121–152, doi: 10.1016/S0377-0273(03)00196-3.

Sharp, R.P. (1973), Mars: fretted and chaotic terrains, Journal of Geophysical Research 78(20), 4073–4083, doi:10.1029/JB078i020p04073

Sheridan, M. F., and K. H. Wohletz (1983), Hydrovolcanism: Basic considerations and review, J. Volcanol. Geotherm. Res., 17, 1–29, doi:10.1016/0377-0273(83)90060-4.

Skinner, J. A., and A. Mazzini (2009), Martian mud volcanism: Terrestrial analogs and implications for formational scenarios, Marine and Petroleum Geology, 26(9), 1866–1878, doi:10.1016/j.marpetgeo.2009.02.006.

Smith, D. E. et al., (2001), Mars Orbiter Laser Altimeter: Experiment summary after the first year of global mapping of Mars, Journal of Geophysical Research, 106 (E10), 23689–23722, doi: 10.1029/2000JE001364.

Valentine, G. A., D. Kier, F. V. Perry, and G. Heiken (2005), Scoria cone construction mechanisms, Lathrop Wells volcano, southern Nevada, USA, Geology, 33, 629–632, doi: 10.1130/G21459AR.1.

Vanderkluysen, L., A.J.L. Harris, K. Kelfoun, C. Bonadonna, and M. Ripepe (2012), Bombs behaving badly: unexpected trajectories and cooling of volcanic projectiles. Bulletin of Volcanology, 74 (8), http://dx.doi.org/10.1007/s00445-012-0635-8.

Wilson, L., and J. W. Head (1994), Review and analysis of volcanic eruption theory and relationships to observed landforms, Reviews of Geophysics, 32, 221–263. doi:10.1029/94RG01113.

Wilson, L., and J. W. Head (2007), Explosive volcanic eruptions on Mars: tephra and accretionary lapilli formation, dispersal and recognition in the geological record, Journal of Volcanology and Geothermal Research, 163, 83–97, doi: 10.1016/j.jvolgeores.2007.03.007.

Wohletz, K. H., and M. F. Sheridan (1983), Hydrovolcanic explosions II. Evolution of basaltic tuff rings and tuff cones, Am. J. Sci., 283, 385–413, doi:10.2475/ajs.283.5.385.

Wood, C.A. (1979), Cinder cones on Earth, Moon and Mars, Lunar Planet, Sci. X, 1370–1372 (abstract).

Wood, C. A. (1980), Morphometric evolution of cinder cones, Journal of Volcanology and Geothermal Research, 7, 387–413, doi: 10.1016/0377-0273(80)90040-2.

Zuber, M. T., D. E. Smith, S. C. Solomon, D. O. Muhleman, J. W. Head, J. B. Garvin, J. B. Abshire, and J. L. Bufton (1992), The Mars Observer Laser Altimeter investigation, Journal of Geophysical Research, 97, 7781–7797, doi:10.1029/92JE00341.

Figures

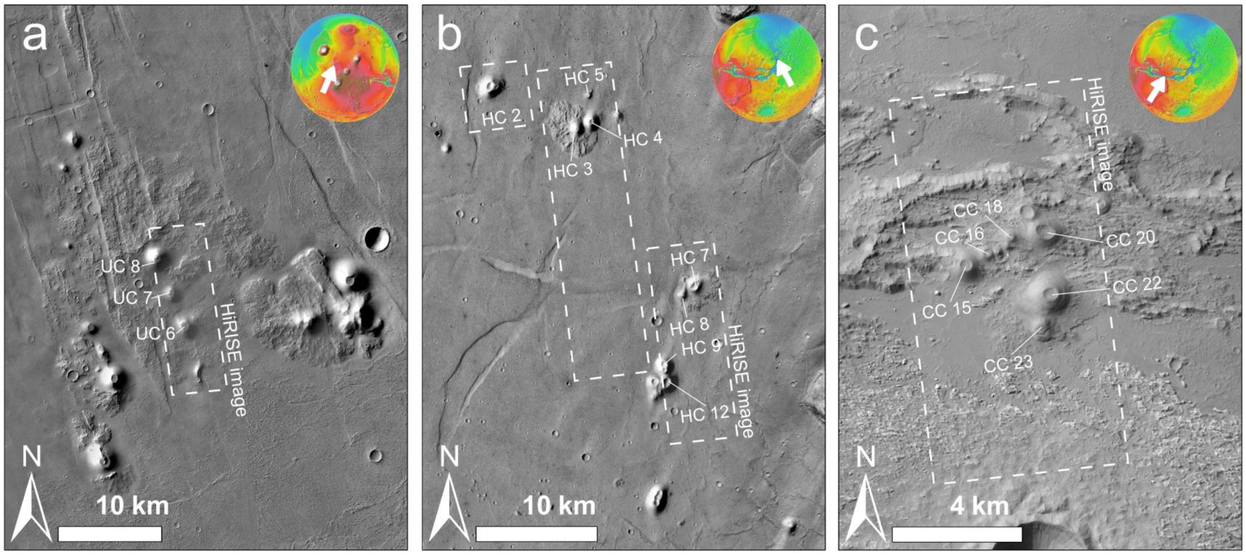

Figure 1

Positions of investigated scoria cones in a) Ulysses Colles (UC), b) Hydraotes Colles (HC), and c) an unnamed field in Coprates Chasma (CC). The boundaries of HiRISE images are marked by dashed white lines. Small insets in the upper right show positions of the volcanic fields on global MOLA topography. Panel a) is based on mosaic of CTX images P21_009409_1858_XN_05N122W, G11_022582_1863_XN_06N122W and P19_008262_1862_XN_06N123W; dashed white outlines indicate HiRISE image PSP_009554_1860 forming stereo-pair with PSP_009409_1860, centered 5.86°N, 237.22°E; panel b) Dashed white outlines indicate HiRISE images ESP_019269_1805, ESP_021458_1800 and ESP_017634_1800 (from west to east) forming stereo-pairs with ESP_019124_1805, ESP_013177_1800 and ESP_025493_1800 respectively, based on mosaic of CTX images G19_025493_1800_XN_00N033W and G02_019124_1803_XN_00N034W centered 0.03°N, 326.26°E; and panel c) Dashed white outlines indicate HiRISE image ESP_034131_1670 forming stereo-pair with ESP_033986_1670, based on CTX image D01_027538_1674_XN_12S062W, centered 12.73°S, 297.21°E.

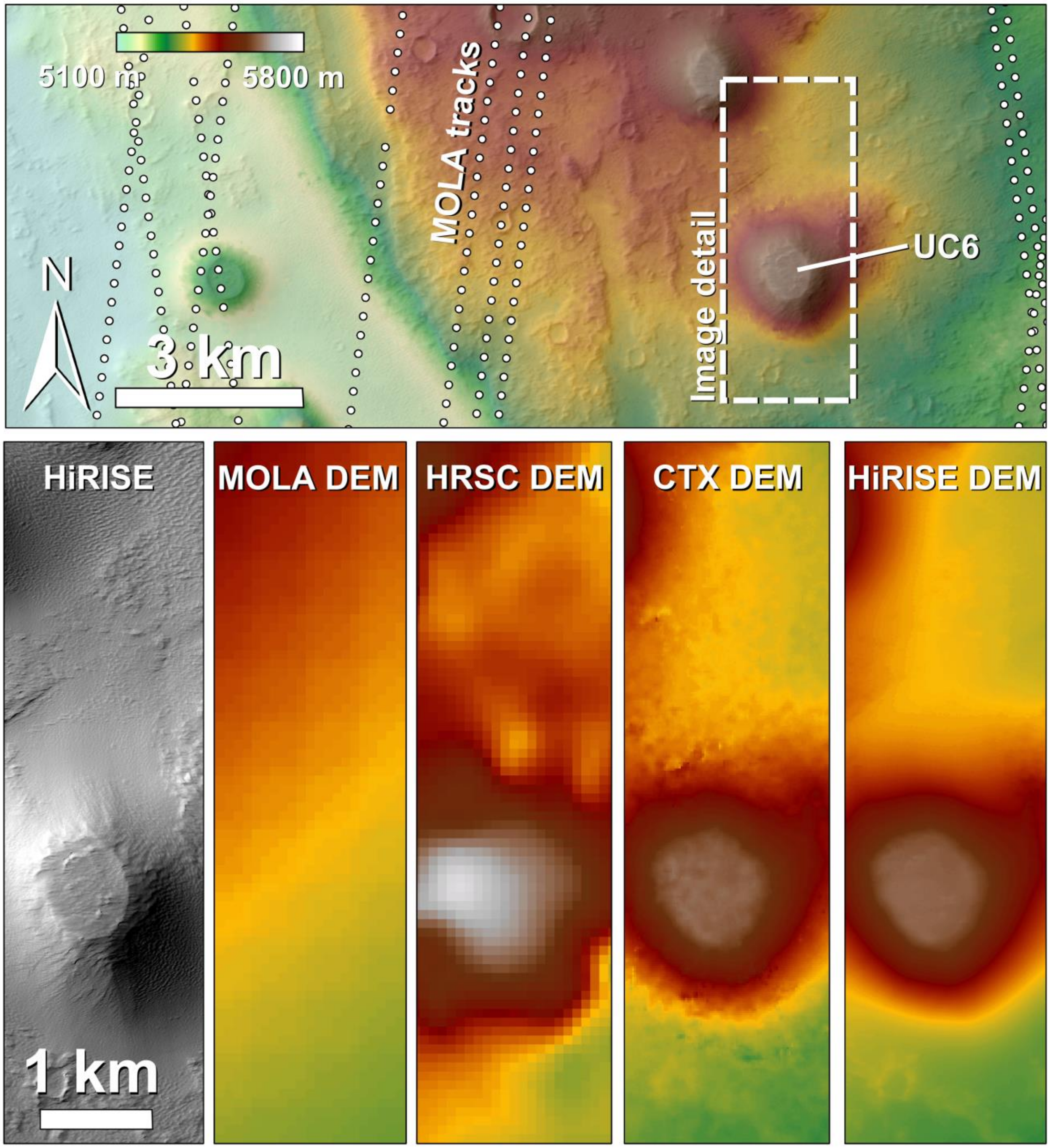

Figure 2

Resolution of various DEMs. The top panel shows the regional context around one particular cone (UC6) in the Ulysses Colles region. The MOLA tracks are marked by white dotted lines. The most detailed topographic information is obtained from the HiRISE DEM.

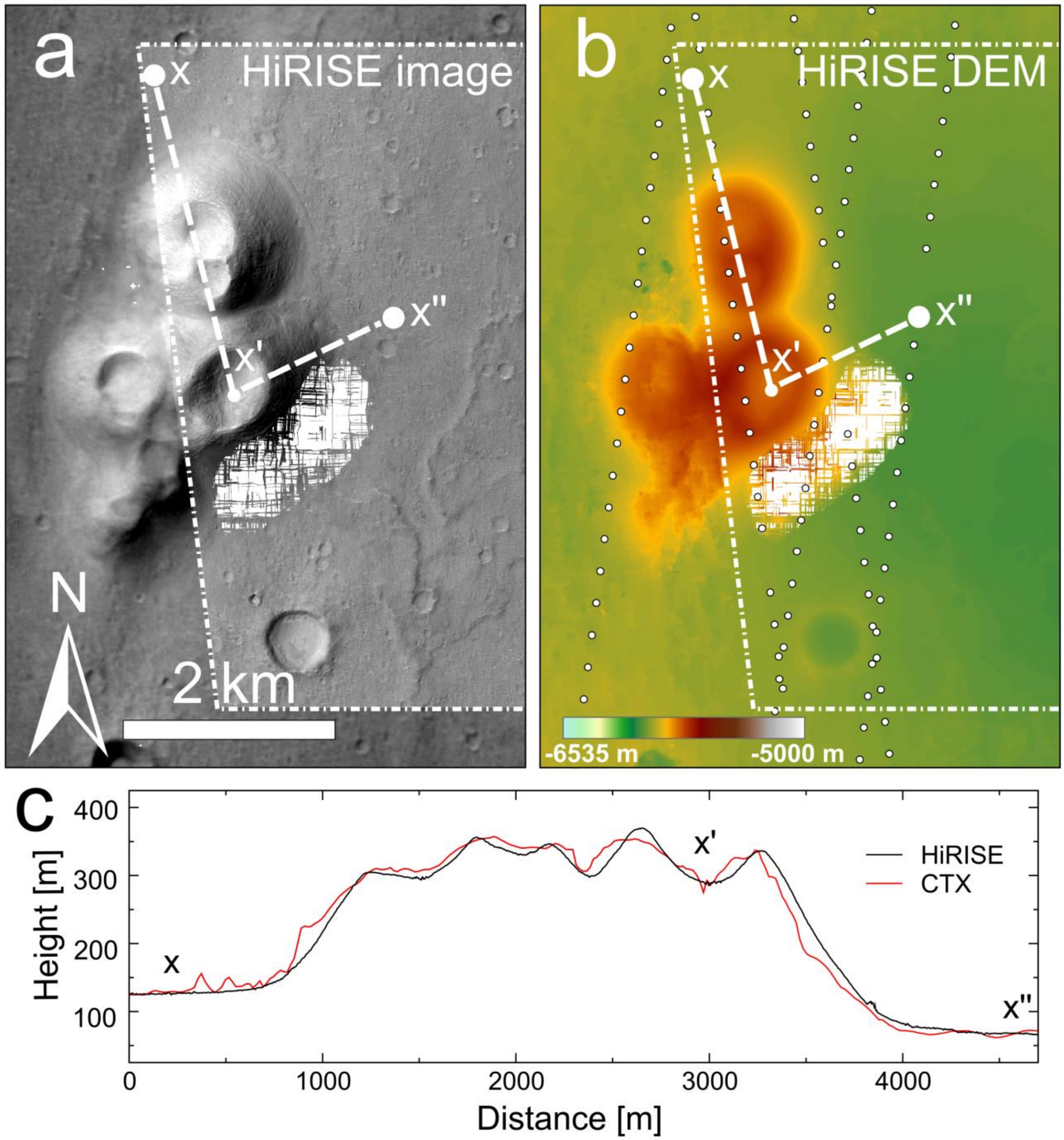

Figure 3

Cones HC9-14 in a) HiRISE and CTX images and b) DEM color mosaic (white dots indicate position of MOLA PEDRs). Resultant DEMs contain data gaps (marked in white on both panels) which do not allow the shapes of some cones to be determined along their entire perimeter. Panel

c) illustrates the differences between profile in the HiRISE and CTX DEMs. Position of the profile connecting points x and x'' is shown in panels a and b. Image center is at 0.13°S, 326.25°E.

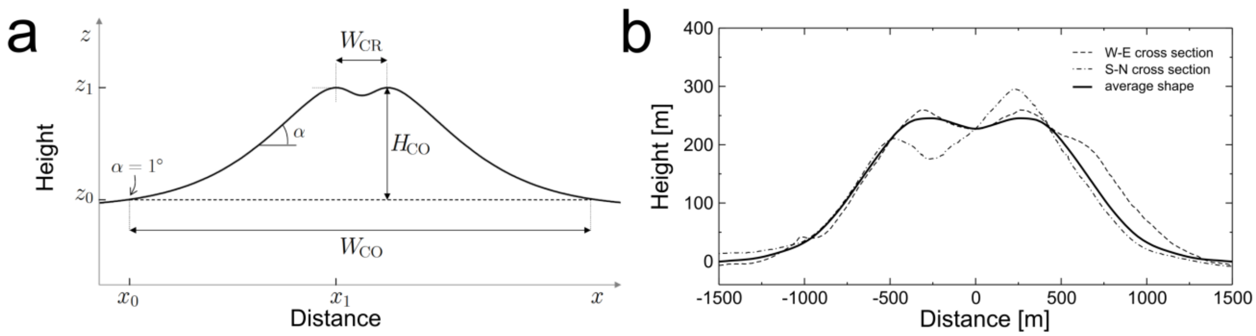

Figure 4

a) Morphometric parameters used in this study. b) Comparison of two profiles passing through the center of the cone HC2 (dashed and dashed-dotted lines) with the average shape of the same cone (full line). The profiles are based on a HiRISE DEM.

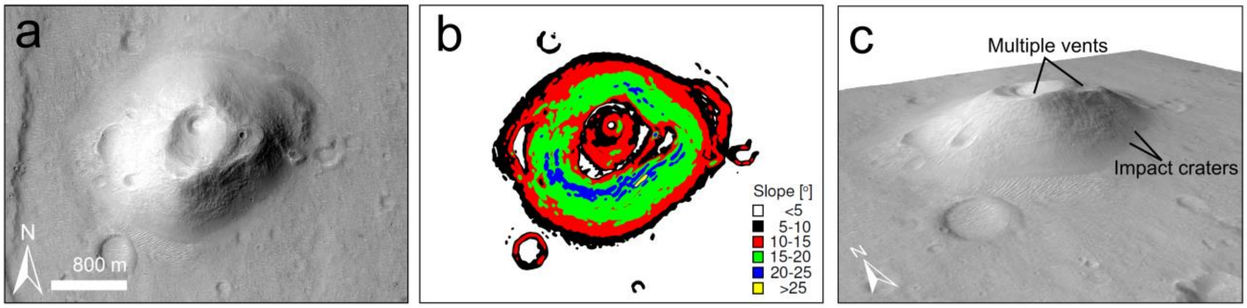

Figure 5

a) Cone HC2 in a HiRISE image ESP_019269_1805, centered 0.26N, 326.04°E. b) Slope map of the same cone. Note that the slope only rarely exceeds 20°. c) A perspective view.

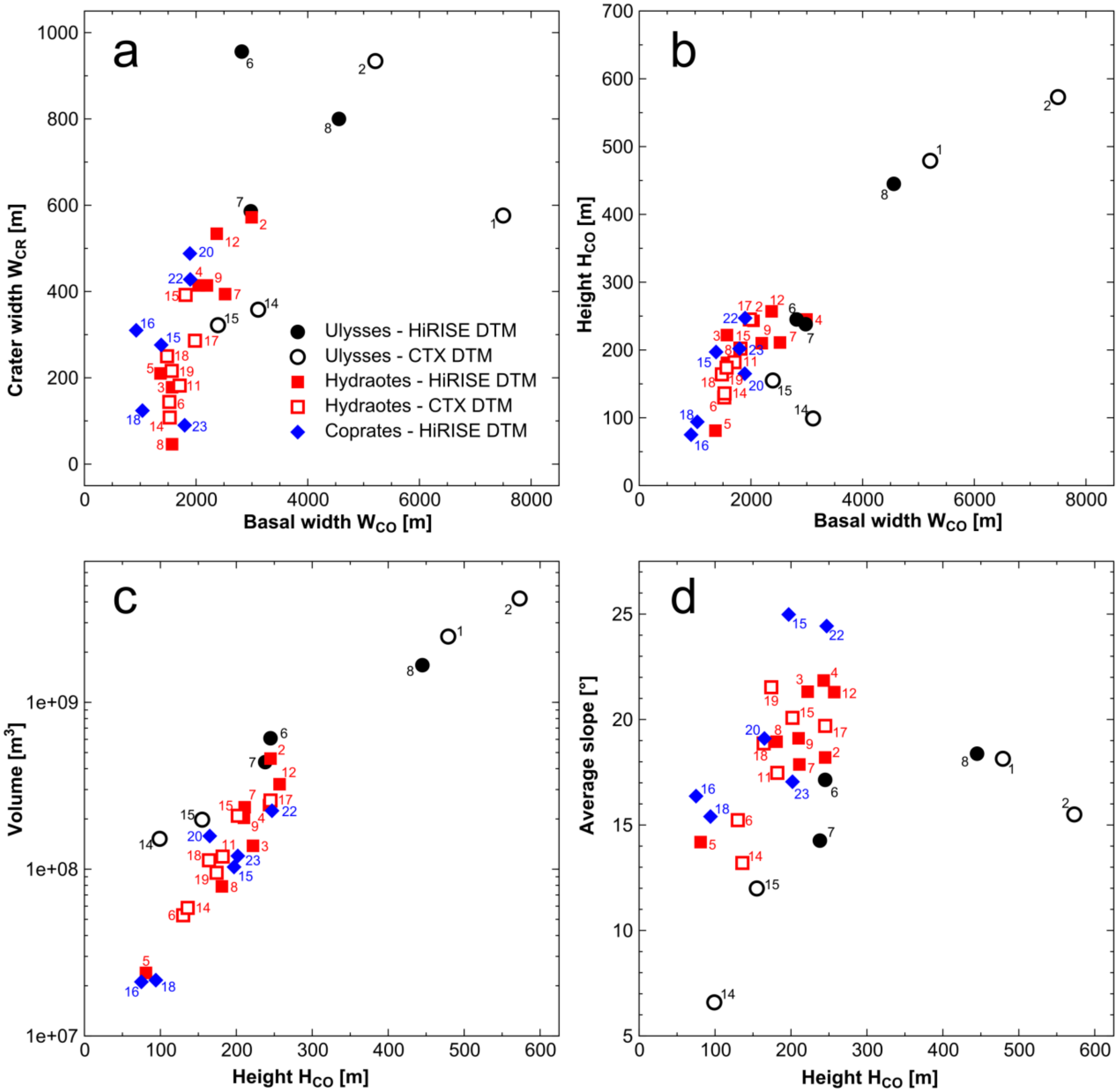

Figure 6

Values of morphometric parameters obtained for average shapes of the 28 cones considered in this study. Full symbols represent HiRISE while empty symbols correspond to CTX DEMs. The results obtained for the UC, HC and CC regions are marked in black, red and blue, respectively.

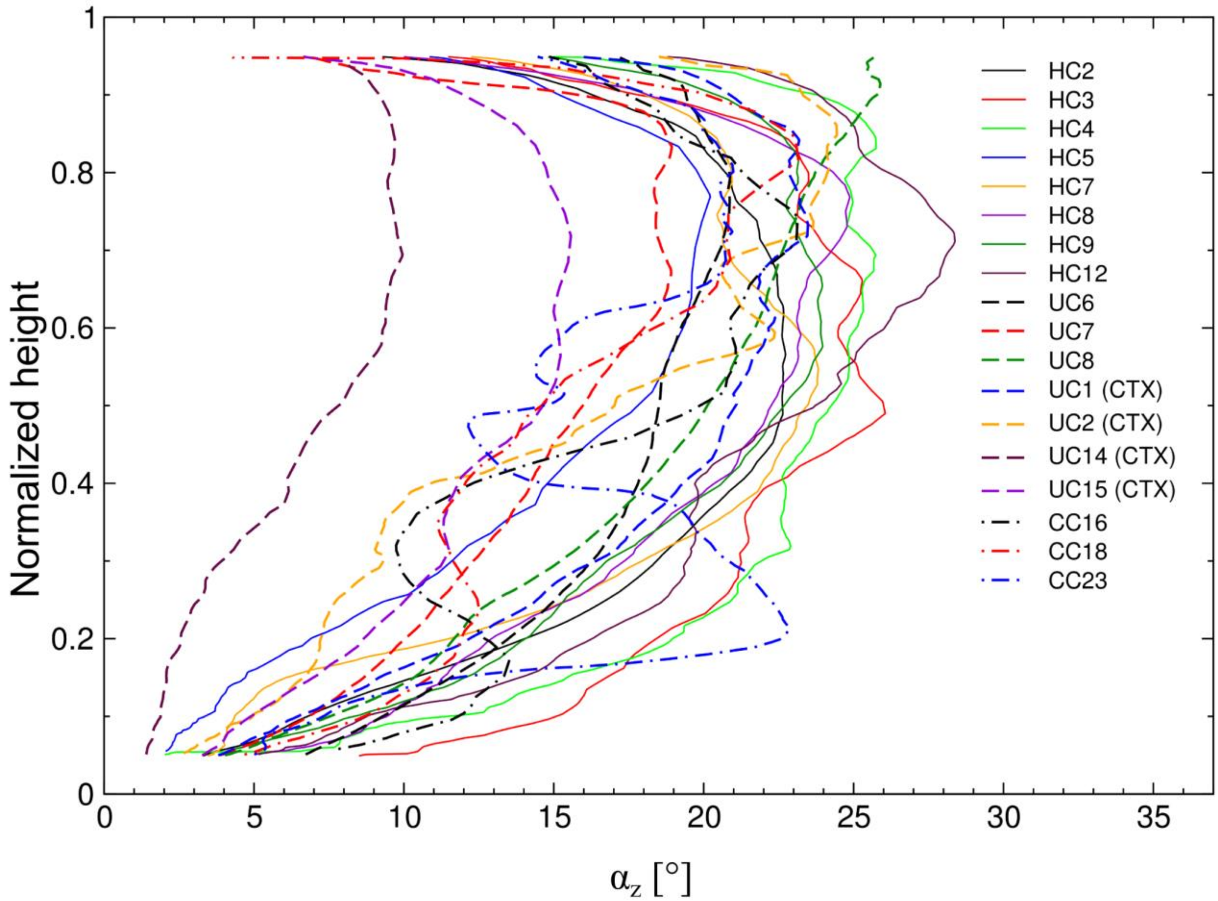

Figure 7

Slope α_z, eq. (1), as a function of normalized height h, plotted for selected cones in HC (full lines), UC (dashed lines) and CC (dash-dotted lines). The curves are computed from HiRISE data, unless stated otherwise.

744

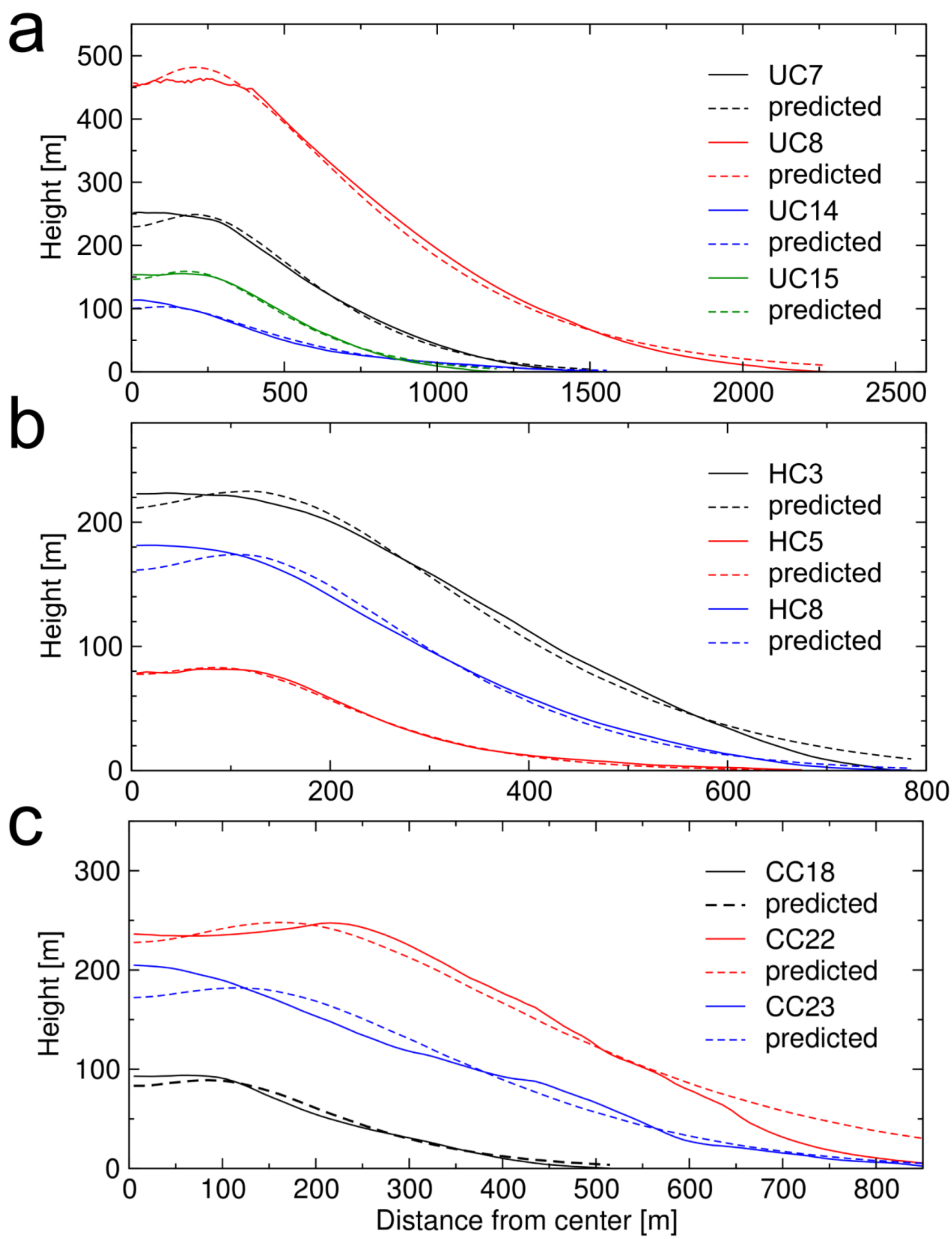

745 ***Figure 8***

Comparison of the average shapes of selected cones in a) UC, b) HC and c) CC (full lines) and the results of numerical ballistic modeling obtained for the same cones (dashed lines). Note that in some cases the model predicts the observed profile with a vertical error smaller than 10 m.

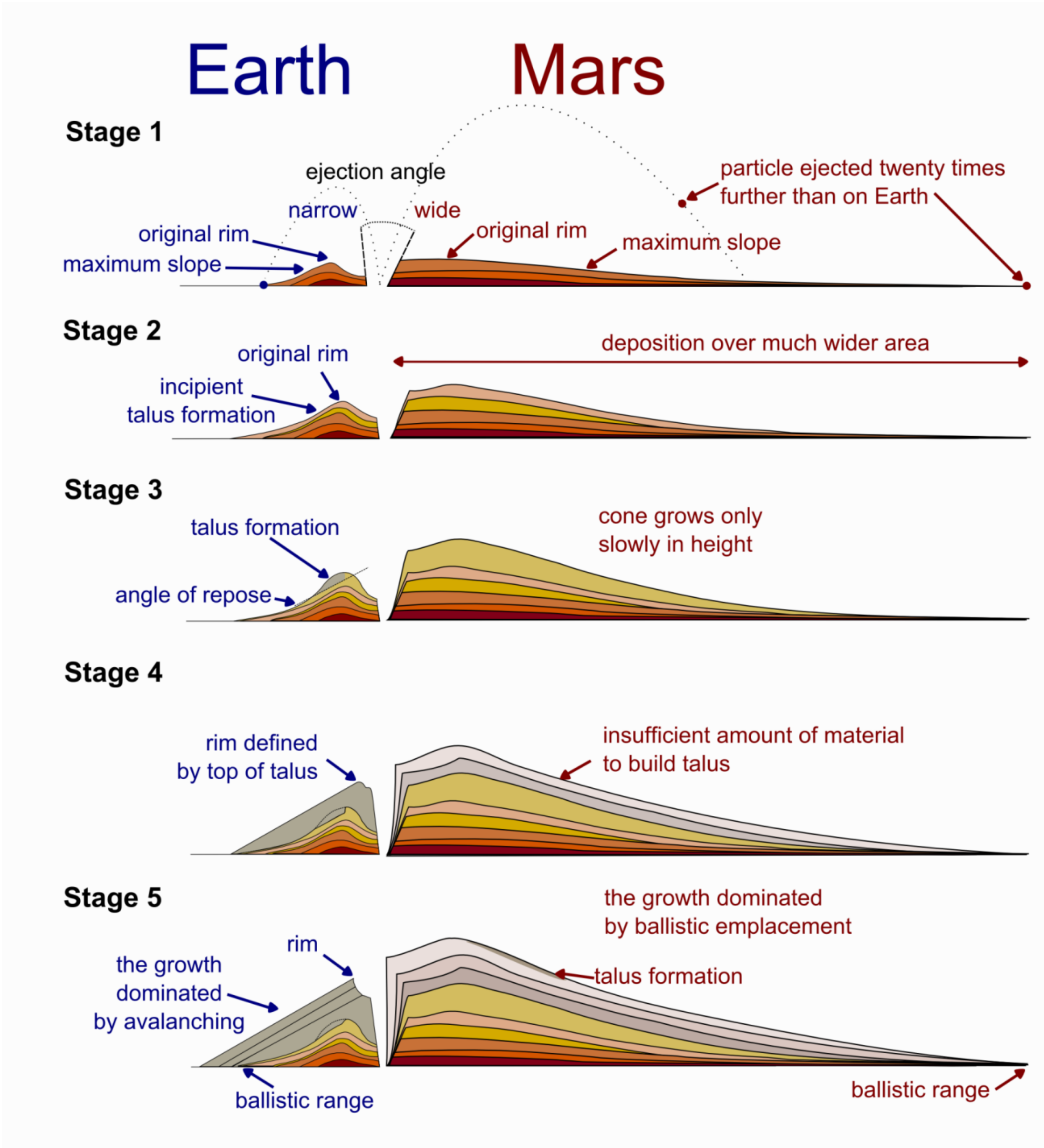

Figure 9

A sketch of scoria cone growth on Earth (after [*McGetchin et al*., 1974]) and on Mars (based on [*Brož et al.,* 2014], and this study).

ID	W_{CR} [m]	W_{CO} [m]	H_{CO} [m]	Volume [m^3]	Average slope [°]	Maximum slope [°]	HiRISE (H) or CTX (C) DTM	Azimuth* [°]	W_{CR}/W_{CO}	H_{CO}/W_{CO}	Initial speed of ejected particles [m/s]	Size of ejected particles [mm]	Match [m]
							Ulysses Colles						
UC1	934	5210	479	2.50E+09	18	24	C	45-90; 225-300	0.18	0.09	110	2	14.2
UC2	576	7500	573	4.20E+09	16	24	C	105-150; 210-265	0.08	0.08	101	4	12.4
UC6	956	2818	245	6.10E+08	17	21	H	135-225	0.34	0.09	138	1	21.8
UC7	586	2980	238	4.40E+08	14	19	H	60-135	0.20	0.08	120	1	6.5
UC8	800	4558	445	1.70E+09	18	26	H	75-180	0.18	0.10	92	2	9.5
UC14	358	3112	99	1.50E+08	7	10	C	0-360	0.12	0.03	64	2	3.2
UC15	322	2392	155	2.00E+08	12	16	C	0-360	0.13	0.06	92	1	3.0
							Hydraotes Colles						
HC2	572	2994	245	4.60E+08	18	23	H	0-360	0.19	0.08	129	2	12.3
HC3	178	1570	222	1.40E+08	21	26	H	180-260	0.11	0.14	120	1	6.1
HC4	414	2046	243	2.40E+08	22	26	H	315-355	0.20	0.12	83	2	11.0
HC5	210	1364	81	2.40E+07	14	20	H	185-355	0.15	0.06	55	1	1.2
HC6	144	1522	130	5.30E+07	15	24	C	225-90	0.09	0.09	46	2	4.0
HC7	394	2520	211	2.40E+08	18	24	H	270-90	0.16	0.08	83	2	6.6
HC8	46	1570	181	7.90E+07	19	25	H	180-315	0.03	0.12	83	1	5.1
HC9	414	2194	210	2.00E+08	19	24	H	0-90	0.19	0.10	83	2	7.8
HC11	182	1706	182	1.20E+08	18	24	C	225-315	0.11	0.11	129	1	4.5
HC12	534	2370	257	3.20E+08	21	28	H	45-60	0.23	0.11	101	2	13.9
HC14	108	1528	136	5.90E+07	13	24	C	0-360	0.07	0.09	46	5	5.5
HC15	392	1812	202	2.10E+08	20	34	C	330-60	0.22	0.11	83	2	12.4
HC17	286	1980	245	2.60E+08	20	32	C	150-240	0.14	0.12	83	2	10.5
HC18	250	1480	164	1.10E+08	19	29	C	0-360	0.17	0.11	138	1	8.0
HC19	216	1564	174	9.50E+07	22	29	C	0-360	0.14	0.11	101	1	7.3
							Coprates Chasma						
CC15	276	1376	197	1.00E+08	25	not determined	H	340-20; 150-225	0.20	0.14	101	1	8.3
CC16	310	928	75	2.10E+07	17	23	H	315-45	0.33	0.08	55	1	4.2
CC18	124	1040	94	2.20E+07	15	23	H	135-180; 290-350	0.12	0.09	55	1	4.0
CC20	488	1890	165	1.60E+08	19	not determined	H	45-225	0.26	0.09	83	2	11.7
CC22	428	1896	247	2.20E+08	24	not determined	H	270-90	0.23	0.13	83	2	15.5
CC23	90	1796	202	1.20E+08	17	23	H	135-225	0.05	0.11	129	1	10.0

* azimuth is measured clockwise with 0° as north

Table 1

Morphometric characteristics of the cones.

Table 2

Key parameters used for modeling of scoria cones on Mars, modified from *Brož et al*. [2014].